A C-BAND MICROWAVE DIELECTRIC PROBE FOR IN-SITU DETECTION OF SOIL MOISTURE

Kasra Barkeshli
Department of Electrical Engineering and Computer Science
University of Michigan
Ann Arbor, MI 48109-2122

May 16, 1985

Abstract

A C-BAND MICROWAVE DIELECTRIC PROBE
FOR IN-SITU DETECTION OF SOIL MOISTURE

A dielectric probe for in-situ moisture detection of materials, comprising an open-ended coaxial line as the sensor mounted on a microstrip circuit board operating at 5 GHz, is described.

A complete model was developed to characterize the coaxial sensor as a short monopole with a complex admittance. The method is based on relating the variations in the permittivity of the material under study to the complex reflection coefficient off the sensor. It offers some unique advantages over conventional techniques including:

- The ability to perform in-situ moisture measurements,
- Elimination of the need for sample preparation and processing in the laboratory, and
- Repeatable data collection and analysis on an almost real-time basis.

The last feature mentioned above makes the probe suitable for estimation of the spatial variability of moisture when studying soil fields.

The system precision for prepared samples was found to be better than 5% for soils of different clay contents. A good agreement between the probe measurements and the theoretical system response was obtained.

A series of field measurements were also conducted to estimate the moisture content of a number of soil types at different sites using the laboratory measurements as calibration data. These sites included soil fields in Lawrence, Kansas as well as Macomb, Illinois–a major site studied during the Shuttle Imaging Radar (SIR-B) mission in 1984.

ACKNOWLEDGEMENTS

This work was supported in part by the National Aeronautics and Space Administration Grant NAG 5-272 under the direction of Professor F. T. Ulaby. The author is grateful to Dr. D. R. Brunfeldt of Applied Microwave Corporation for his technical assistance.

Contents

List of Figures

List of Tables

Chapter 1

INTRODUCTION

The motivation for permittivity measurement of materials is of vital importance in microwave remote sensing, since the interaction of electromagnetic energy with substances depends on their permittivity. Fundamental study of materials along with quantitative dielectric data are to be used as input to mathematical models, which could then result in an insight into emission and scattering problems. The complex permittivity ε, influences the radar scattering coefficient through Fresnel reflection coefficient and attenuation constant by defining the skin depth. Also in the inverse problem, it is of great importance in target discrimination and identification.

The permittivity of wet soil, as that of other moist materials, is a strong function of its moisture content in a wide frequency range. However the routine sampling and treatment of soils for moisture determination is time consuming and in most cases tedious. Moreover, it is not certain to what extent the prepared samples are representative of soils as they exist in the field because the lab-processing techniques can significantly alter the electrical properties of the soil.

In recent years a considerable amount of effort has been made on the development of different types of dielectric measurement schemes for in-situ determination of permittivity and moisture content of materials [1]-[3]. In general the invasive techniques which involve immersing a sensor into the medium give more sensitive responses to dielectric variations as opposed to non-invasive techniques.

An open-ended coaxial line has been used as a sensor in measurement of biological substances and lossy dielectrics at radio and microwave frequencies based on reflection method [3].

This report is concerned with a simple measurement system which utilizes open-ended coaxial lines for in-situ detection of soil moisture. A portable C-band dielectric probe was developed and used to study the within-field spatial variation of moisture in agricultural fields [4]. After a brief review of the dielectric behavior of wet soils, the equivalent model for the probe and the principle of operation are introduced. Calibration methods and design considerations are presented next. The measurement set up and the experimental results are also discussed.

Chapter 2

Soil Parameters

The complex permittivity of soil is a function of moisture content m, particle size distribution $p(r)$[1], bulk density ρ_b, salinity s, temperature T, and frequency f [5]

$$\varepsilon = \mathcal{F}(m, p(r), \rho_b, s, T; f) \tag{2.1}$$

In the following sections,we briefly review the contributions of these parameters to soil permittivity.

2.1 Soil moisture

Soil moisture has the greatest effect on the permittivity of wet soil. The structure of water molecules gives rise to a space charge distribution which can be thought of as an electric dipole. The relaxation frequency of water lies in the microwave region. Thus, when placed in an electromagnetic field, the dipolar relaxation of water molecules results in an absorption of the microwave energy which can be used as a measure of soil moisture content [6].

[1] Also referred to as texture.

Typically, the relative permittivity of water is $\epsilon_{H_2O} = 80 - j17$, while that of dry soil is $\epsilon_{\text{dry soil}} = 2.4 - j0.01$. Therefore, since the permittivity of pure water is much larger than that of dry soil, the permittivity of the mixture is dominated by that of water.

Since it is the number of the polarized dipole moments per unit volume that determines the dielectric contribution of water, volumetric water content rather than the gravimetric moisture content (percent by weight) is preferred in dielectric measurements. It is observed (Figure 2.1) that the scatter in dielectric data due to soil density for gravimetric moisture is drastically minimized when data is plotted against volumetric moisture content [4]. For soil samples of known volume, the volumetric moisture content m_v, is defined as

$$\begin{aligned} m_v &= \frac{W_{H_2O}}{W_{\text{dry soil}}} \cdot \frac{\rho_{\text{soil}}}{\rho_{H_2O}} \quad , \quad gr/cm^3 \\ &= m_g \cdot \rho_b \end{aligned} \tag{2.2}$$

where W denotes the weight and m_g and ρ_b are gravimetric soil moisture and soil bulk density, respectively.

2.2 Texture

The complex permittivity of soil as a function of moisture content displays a dependence on its texture. Figure 2.2 shows the variation of the relative permittivity as a function of textural composition for five different soils in Lawrence, Kansas as listed in Table 2.1. This dependence is attributed to moisture holding capacity of soils which is directly related to their total surface area through particle size

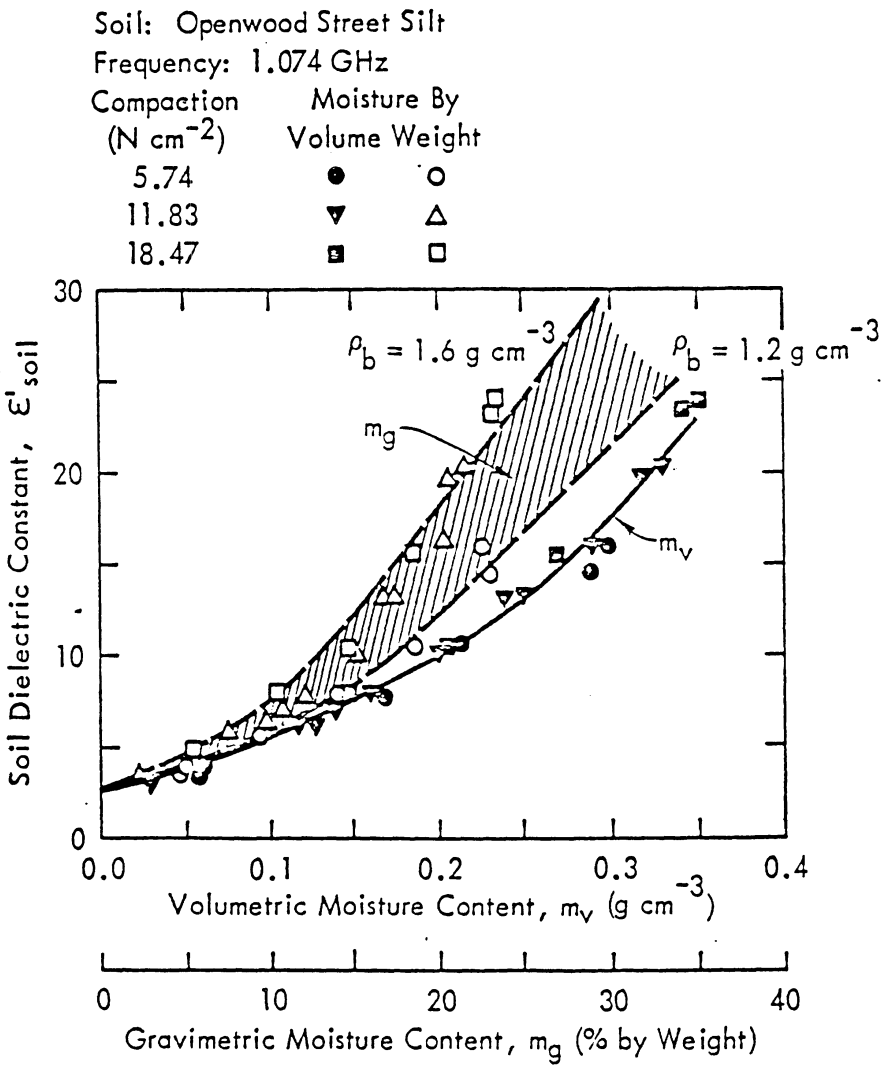

Figure 2.1: Change in relative dielectric constant due to soil moisture units used (from Cihlar and Ulaby, 1974; based on data from Lundien, 1971).

SOIL		SOIL TEXTURE %		
TYPE		SAND	Silt	Clay
1	Sandy Loam	51.1	35.06	13.43
2	Loam	42.0	49.5	8.5
3	Silt Loam I	30.63	55.89	13.48
4	Silt Loam II	17.16	63.84	19.00
5	Silty Clay	5.02	47.60	47.38

Table 2.1: Soil classification of five fields in Lawrence, Kansas.

distribution. Since clay particles have very large surface area per unit weight, soils with significant clay content can retain a high level of moisture before reaching saturation. Figure 2.3 shows the two states at which water molecules are held among soil particles. The fine clay particles coating the soil solids tightly absorb water in the form of bounded molecules while the capillary forces are responsible for the free water present in the soil sample which contributes the most to the soil permittivity. Hence, in general one would expect less dielectric sensitivity to moisture variations for soils containing higher clay fractions especially at lower moisture contents due to absorption of water at the surface of fine particles and absence of free water molecules.

The effect of texture on permittivity is reduced as we go higher in frequency.

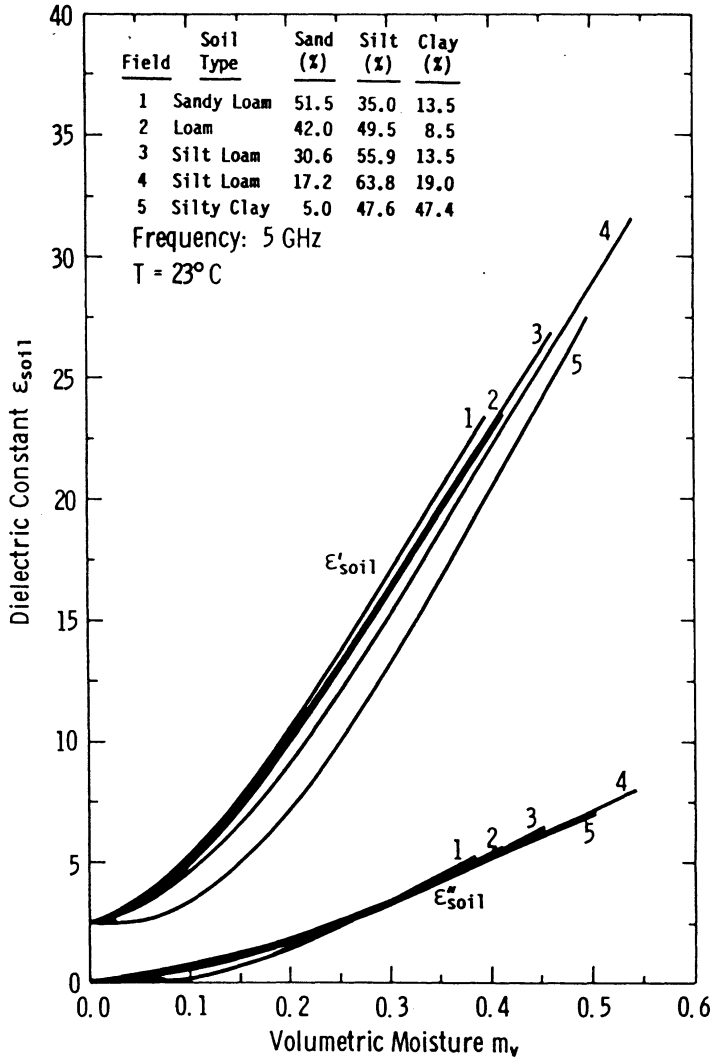

Figure 2.2: Measured relative permittivity for five soils at 5 GHz. The textural composition of the soils are listed in Table 2.1.

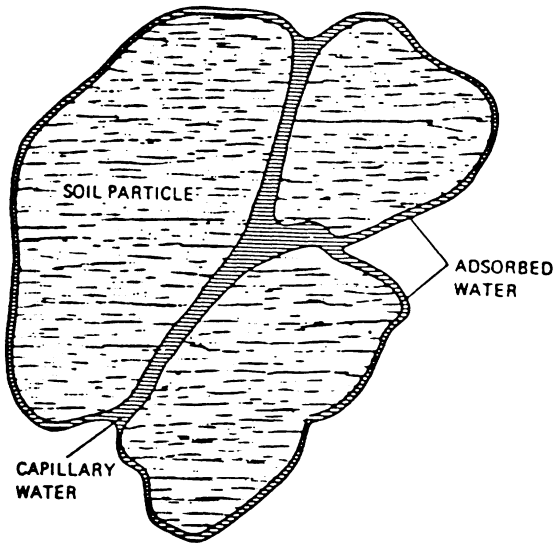

Figure 2.3: The two states of water in wet soil.

2.3 Bulk Density, Salinity, and Temperature

Bulk density affects the relationship between permittivity and soil moisture content in an indirect manner. However, from Figure 2.1 it is apparent that when moisture content is expressed on a volume basis, the uncertainty introduced by bulk density in the dielectric constant of soils of the same type almost disappears.

Conductivity $\sigma = \omega\epsilon''$ is a strong function of salinity. This dependence becomes weak at microwave frequencies above C-Band. Also, for dry soil, the dielectric constant is essentially independent of temperature. The permittivity of wet soil, on the other hand, is a function of temperature due to the presence of water molecules. This dependence, however, is very weak above 0°C [4].

Chapter 3

PRINCIPLE OF OPERATION

The system's operation is based on relating the permittivity variations of the medium to the complex reflection coefficient off an open-ended coaxial transmission line immersed in the material under study. Figure 3.1 shows the geometry of the sensor.

The complex reflection coefficient off the sensor terminated in a medium of relative permittivity ϵ is defined as

$$\Gamma = \frac{Z_L(\epsilon) - Z_c}{Z_L(\epsilon) + Z_c} = \frac{Y_c - Y_L(\epsilon)}{Y_c + Y_L(\epsilon)} \tag{3.1}$$

where Z_L and Y_L are the load impedance and load admittance and Z_c and Y_c are the characteristic impedance and characteristic admittance of the line, respectively.

3.1 Sensor Equivalent Circuit in Free Space

An open-ended coaxial line can be regarded as a short monopole whose terminal admittance in free space ($\epsilon_0 = 1$) is given by [7]:

$$Y_L(\epsilon_0) = G_0 + j\omega C_T \tag{3.2}$$

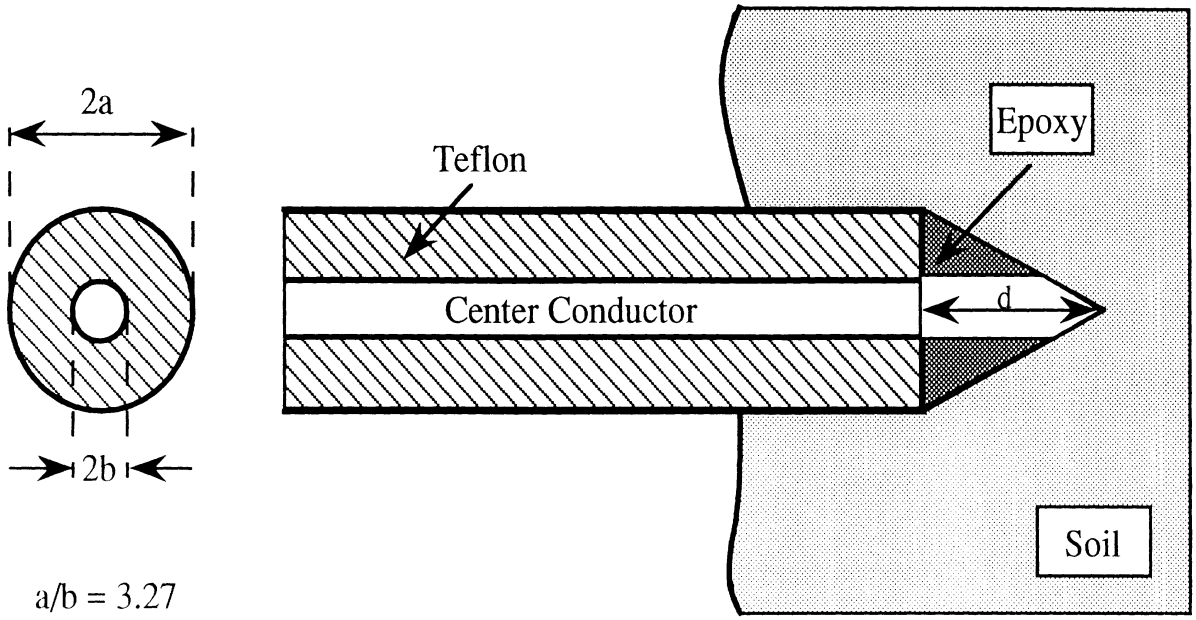

a/b = 3.27

$d/\lambda << 1$

Equivalent Circuit in Free Space

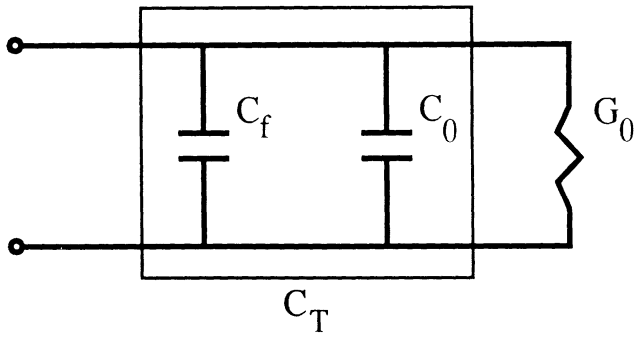

Figure 3.1: Geometry of the coaxial sensor and its equivalent circuit.

a, in.	C_T, pf
0.085	0.016
0.141	0.027
0.250	0.041

Table 3.1: Total capacitance for some semi-rigid coaxial lines ($a/b = 3.27$) [8].

where G_0 and C_T are determined by the physical dimensions of the line and account for the radiation loss and reactive impedance of the monopole, respectively.

The total capacitance C_T is a combination of two components:

$$C_T = C_0 + C_f \tag{3.3}$$

C_0 represents the storage of energy in the dielectric sample, while C_f is the internal capacitance which accounts for the storage of energy in the fringing fields internal to the dielectric filling of the coaxial line and is basically not affected by the presence of the dielectric sample. Numerical analysis of semirigid teflon dielectric lines show that for these lines [8]

$$0.05 \leq C_f/C_0 \leq 0.2 \tag{3.4}$$

The total capacitance C_T is related to the inner and outer radii of the line and Table 3.1 lists the total capacitance for three standard coaxial cables ($a/b = 3.27$) in free space [9].

In Equation 3.2, G_0 represents losses due to radiation. For an air-field coaxial

Geometry		$f = 5$ GHz			$f = 10$ GHz		
a, in.	A	a/λ	$(a-b)/\lambda$	$G_0, \mho$	a/λ	$(a-b)/\lambda$	$G_0, \mho$
0.085	2.18×10^{-48}	0.036	0.025	2.12×10^{-6}	0.072	0.050	3.39×10^{-5}
0.141	1.43×10^{-47}	0.060	0.054	1.39×10^{-5}	0.120	0.108	2.22×10^{-4}
0.250	1.16×10^{-46}	0.106	0.074	1.13×10^{-4}	0.212	0.147	1.18×10^{-3}

Table 3.2: Calculated conductance for standard semi-rigid cables ($a/b = 3.27$).

line, G_0 is proportional to ω^4

$$G_0 = A\omega^4 \tag{3.5}$$

and at low frequencies where $a/\lambda \ll 1$,

$$A \simeq \frac{Y_c}{24 \ln(a/b)} \left(\frac{b^2 - a^2}{c^2} \right) \quad , \quad \frac{a-b}{\lambda} < 0.1 \quad , \quad a/b \geq 3 \tag{3.6}$$

where Y_c and c are the characteristic admittance of the line and speed of light, respectively. Table 3.2 shows the calculated values of radiation conductance for the lines considered in Table 3.1.

3.2 Equivalent Circuit in Dielectric Medium

Consider the sensor described by Equation 3.2 inserted in a homogeneous medium of relative permittivity ϵ. The input admittance of the line can now be written as

$$Y_L(\epsilon) = G(\epsilon) + j\omega C_T(\epsilon) \tag{3.7}$$

To find the explicit form of the sensor equivalent circuit in this case, we make use of the following antenna modeling theorem [10]

$$Z_L(\omega, \epsilon) = \eta Z_L(n\omega, \epsilon_0) \tag{3.8}$$

where $\eta = \sqrt{\mu/\epsilon}$ is the normalized intrinsic impedance of the medium and $n = \sqrt{\mu\epsilon}$ is the index of refraction. For a nonmagnetic medium ($\mu = 1$), (3.8) reduces to

$$\begin{aligned} Z_L(\omega, \epsilon) &= \frac{1}{\sqrt{\epsilon}} Z_L(\omega\sqrt{\epsilon}, \epsilon_0) \\ Y_L(\omega, \epsilon) &= \sqrt{\epsilon}\, Y_L(\omega\sqrt{\epsilon}, \epsilon_0) \end{aligned} \tag{3.9}$$

Substituting for $Y_L(\epsilon_0)$ from (3.2) and noting that the internal fringing capacitance C_f is not affected by the presence of the dielectric medium, we have

$$\begin{aligned} Y_L(\omega, \epsilon) &= \sqrt{\epsilon}\left[A(\omega\sqrt{\epsilon})^4 + j\omega\sqrt{\epsilon}\, C_0\right] + j\omega C_f \\ &= A\omega^4\epsilon^{2.5} + j\omega(C_0\epsilon + C_f) \end{aligned} \tag{3.10}$$

which is to be compared with (3.7) so that

$$G(\epsilon) = A\omega^4\epsilon^{2.5} \tag{3.11}$$

and

$$C_T(\epsilon) = C_0\epsilon + C_f \tag{3.12}$$

For a medium of known dielectric ($\epsilon = \epsilon' - j\epsilon''$), (3.12) assumes a linear model for the total capacitance as a function of permittivity. The linear model has the advantage that it yields closed-form expressions for the real and imaginary parts of

the relative permittivity in terms of the input reflection coefficient and frequency when radiation loss is negligible (Appendix A).

Substituting (3.12) in (3.1) now yields

$$\Gamma = \frac{Y_c - [A\omega^4\epsilon^{2.5} + j\omega(C_0\epsilon + C_f)]}{Y_c + [A\omega^4\epsilon^{2.5} + j\omega(C_0\epsilon + C_f)]} \tag{3.13}$$

Thus, if the line equivalent circuit components C_f, C_0, and A are known, ϵ of the medium can be recovered from measured values of the reflection coefficient Γ.

3.3 Sensor Calibration

An important step in utilizing any sensor is the accurate estimation of its equivalent circuit components.

For the dielectric probe considered in this study, the equivalent circuit components are determined from the input reflection coefficient measured by a Network Analyzer when dielectrics of well known properties are in contact with the sensor. In so doing the complete model incorporating the radiation loss, as well as the external and internal fringing capacitances, is developed and the contribution of each component to the terminal admittance of the probe is examined. Denoting the complex relative permittivity of the calibrating material as ϵ_c, the measured admittance of the loaded sensor Y_L^m is given by (see (3.10))

$$Y_L^m = G_0\epsilon_c^{2.5} + j\omega(C_0\epsilon_c + C_f) \tag{3.14}$$

which can be expressed as ($\epsilon_c^{2.5} = \xi - j\zeta$)

$$Y_L^m = G_0\xi + \omega C_0\epsilon_c'' + j[-G_0\zeta + \omega C_0(Q + \epsilon_c')] \tag{3.15}$$

where $Q = C_f/C_0$ is specified by (3.4). Solving this equation for C_0 and G_0, we obtain:

$$C_0 = \frac{\zeta \Re\mathrm{e}\{Y_L^m\} + \xi \Im\mathrm{m}\{Y_L^m\}}{\omega[\xi(\epsilon_c' + Q) + \zeta\epsilon_c'']} \tag{3.16}$$

$$G_0 = (\Re\mathrm{e}\{Y_L^m\} - \omega C_0 \epsilon_c'')/\xi \tag{3.17}$$

while

$$C_f = QC_0 \tag{3.18}$$

and $\Re\mathrm{e}\{\cdots\}$ and $\Im\mathrm{m}\{\cdots\}$ denote real and imaginary parts of $\{\cdots\}$. In practice, the input admittance Y_L^m is obtained from the measured reflection coefficient Γ_m as

$$Y_L^m = Y_c \frac{1 - \Gamma_m}{1 + \Gamma_m} \tag{3.19}$$

The calibrating system is a standard reflection measurement setup which utilizes a computer controlled Network Analyzer as described in Appendix B.

Chapter 4

SYSTEM CONFIGURATION

The block diagram of the probe appears in Figure 4.1. The RF section consists of a voltage controlled oscillator (VCO) with an operating frequency range of 4.5 to 5.1 GHz, a 3 dB microstrip hybrid ring, the sensor with accompanying phase shifter and a detector diode which delivers the detected signal to the voltmeter. The dc section includes a rechargeable power supply, a dc-dc converter, the bias and tuning network and a digital panel meter. The entire circuit is enclosed in a portable fiber glass enclosure. The coaxial cable can be extended out for probing the soil at different depths.

4.1 System Transfer Function

Consider an RF signal generated by the oscillator

$$v_i = 2V\cos(\omega t) \tag{4.1}$$

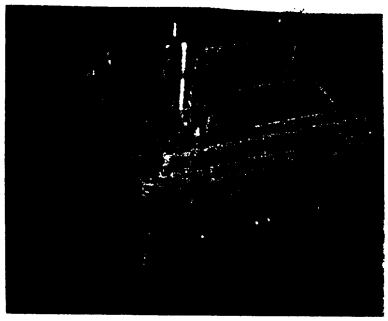

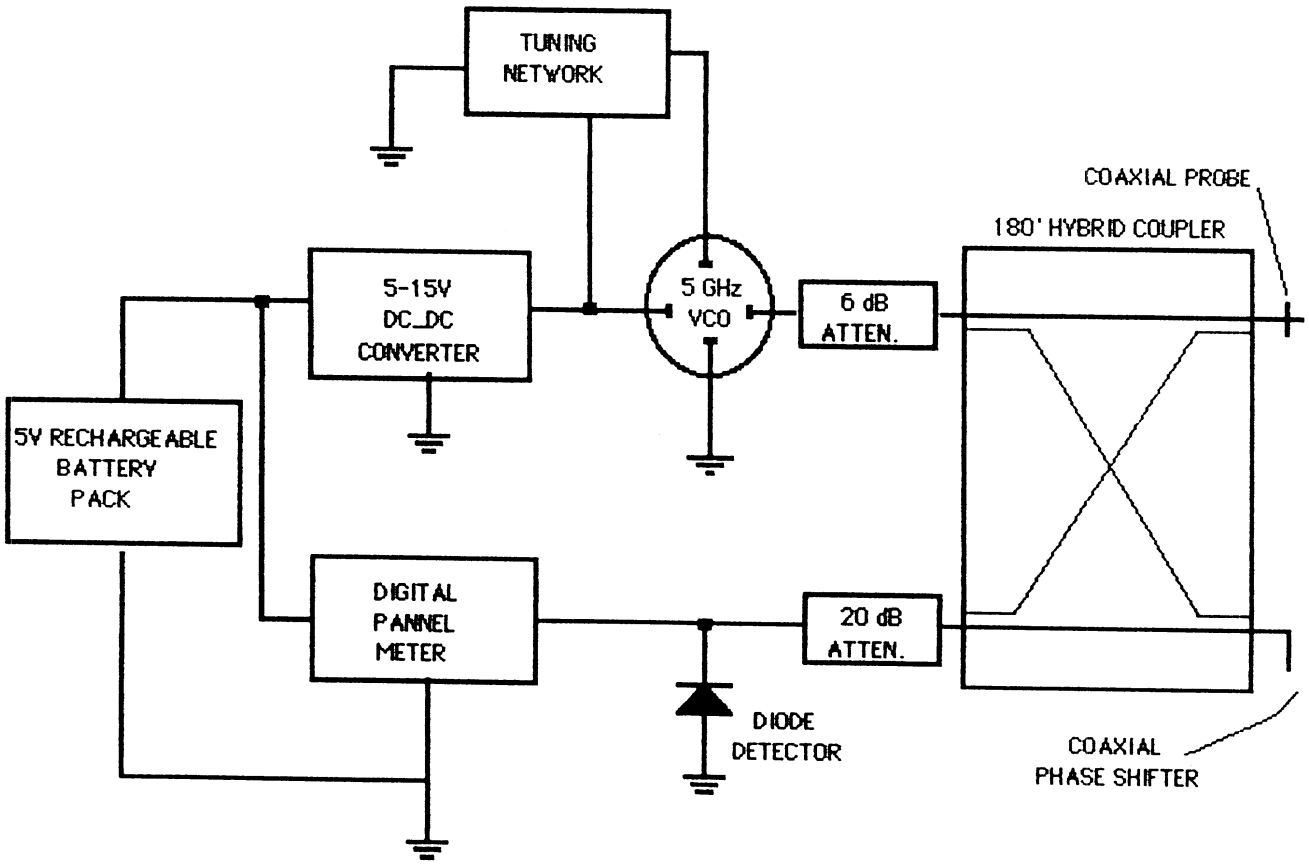

Figure 4.1: The C-band soil moisture probe and its block diagram.

The signal energy is divided in half; one portion (test signal) is directed to the sensor and undergoes reflection by the material under study

$$v_t = V|\Gamma|\cos(\omega t + \phi) \tag{4.2}$$

where $|\Gamma|$ and ϕ are the magnitude and phase of the reflection coefficient. The other portion of the incident energy (reference signal) is coupled through the hybrid ring to a phase shifter (a coaxial cable of comparable length) which is adjusted to compensate for the phase difference due to different path lengths. Thus, we have

$$v_r = V\cos(\omega t) \tag{4.3}$$

The two signals add together out of phase at the output of the coupler and the resultant field is detected by the diode detector which is biased so that it operates in the square law region

$$v_d = k(v_t - v_r)^2 \tag{4.4}$$

where k is a constant. Substituting for v_t and v_r and expanding, we have

$$\begin{aligned} v_d &= k\left[V|\Gamma|\cos(\omega t + \phi) - V\cos(\omega t)\right]^2 \\ &= \frac{kV^2}{2}\left\{1 + \cos(2\omega t) + |\Gamma|^2 + |\Gamma|^2\cos(2\omega t + 2\phi) - 2|\Gamma|[\cos(2\omega t + \phi) + \cos\phi]\right\} \end{aligned} \tag{4.5}$$

The voltmeter responds to the dc component of the detector output, thus eliminating the high frequency components. Therefore, the detected signal is given by

$$v_D = K(1 + |\Gamma|^2 - 2|\Gamma|\cos\phi) \tag{4.6}$$

where $K = \frac{kV^2}{2}$.

Variations in dielectric properties of the soil due to moisture is translated to the amplitude and phase of the reflection coefficient through Equation (3.1) which is in turn detected by the detector according to (4.6). Figure 4.2 shows the normalized transfer function of the probe versus volumetric moisture content for different soil types in Table 2.1. To generate this plot, an empirical polynomial relationship between the permittivity and the moisture content based on experimental results has been used [11,12].

4.2 Design Considerations

The design parameters (frequency of operation, size of the coaxial sensor, etc.) are chosen to optimize the probe response to soil moisture. As mentioned earlier, the effects of soil salinity and texture on its dielectric constant decreases as one goes higher in frequency while the radiation loss increases (Table 3.2). A 0.085 in. coaxial line was chosen with an operating frequency of 5 GHz. At this frequency level, the radiation loss is negligible and the linear model (3.12) is sufficient to model the probe

$$Y_L(\epsilon) = j\omega(C_0\epsilon + C_f) \tag{4.7}$$

Also, by choosing a suitable substrate, a reasonable size for the microstrip circuit was realized. The design steps are discussed in some detail in Appendix C.

Table 4.1 shows the estimated values of the equivalent circuit components for the sensor using the calibration procedure outlined in Section 3.3. These results

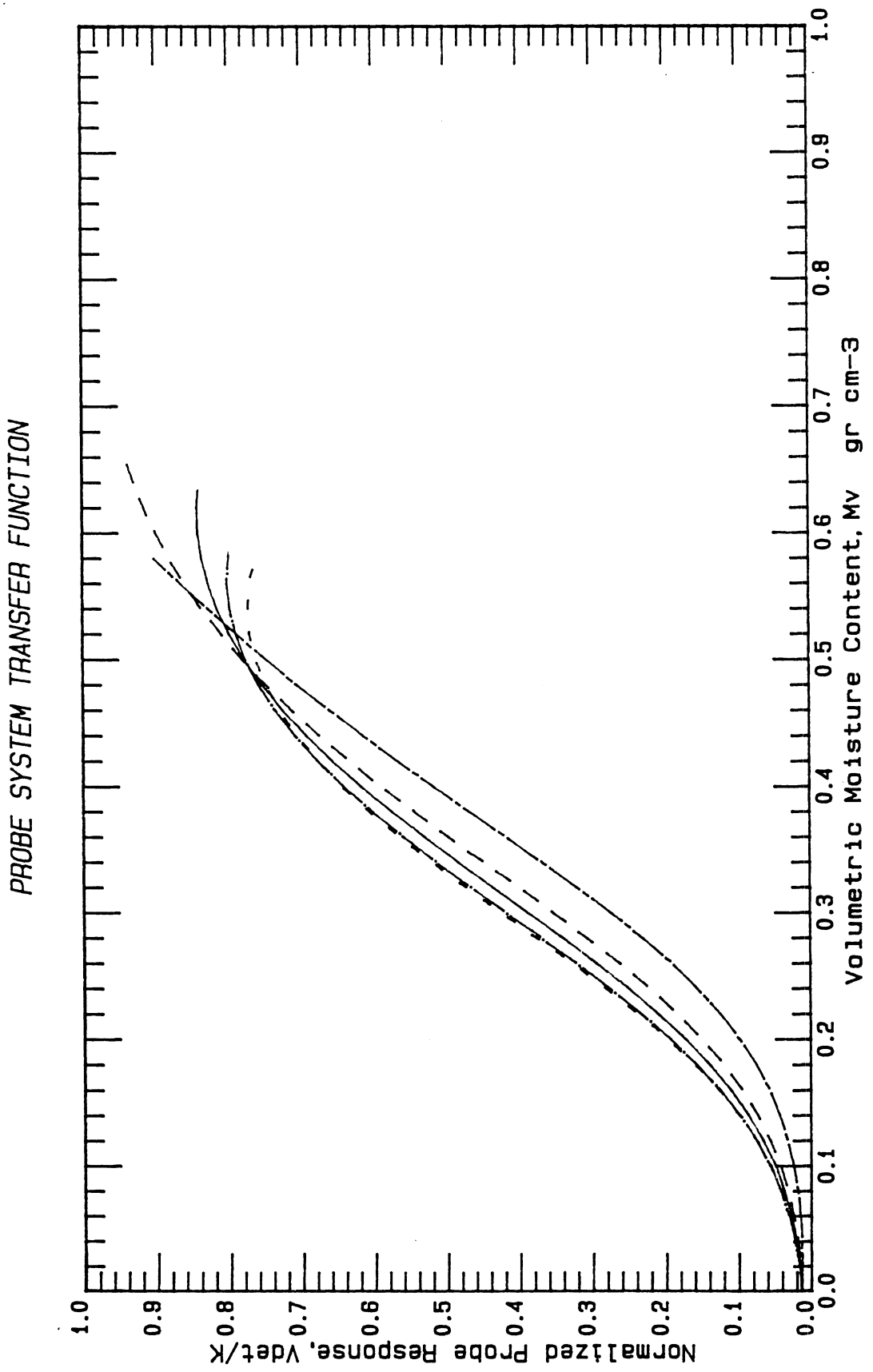

Figure 4.2: The normalized theoretical transfer function of the probe as a function of volumetric moisture content for the soil types listed in Table 2.1.

C_0, pf	C_f, pf	$G_0, \mho$
0.0146	0.001	0.712×10^{-6}

Table 4.1: Estimated values of the equivalent circuit components for the 0.085″ coaxial cable at 5 GHz.

are in good agreement with the theoretical approximations tabulated in Tables 3.1 and 3.2[1]. They will be used later to validate the experimental results obtained by probing soils of various textures.

[1]The ratio $Q = C_f/C_T$ was assumed to be 0.1 in accordance with (3.4).

Chapter 5

EXPERIMENTAL RESULTS

The moisture probe was tested in a series of laboratory and field observations. Figure 5.1 shows the probe response for different types of laboratory prepared soil samples. Immediately after each probe measurement, the moisture content of the sample tested was measured directly using conventional drying techniques. Clearly, the general behavior of the probe is similar to the theoretical transfer function of Figure 4.2. The textural composition of the soils used in this experiment is listed in Table 2.1.

It is observed that as clay content of the soil increases, the probe response shifts in the direction of higher moisture. This is in agreement with the remarks in Section 2.2 and is attributed to the larger surface area per unit weight of clay particles. The solid line in Figure 5.1 is a polynomial fit with a correlation coefficient of 0.98 and gives a maximum error of 0.05 gr/cm^3 in the estimation of volumetric soil moisture *if the soil type is ignored.*

In the Fall of 1984, a number of soil moisture probes were developed at the University of Kansas Center for Research, Inc. to be used in the ground-truth

measurements supporting the SIR-B Space Shuttle mission in October 1984. Figure 5.2 shows the efficiency of the probe in studying the moisture distribution of soils in natural fields. The figure is a histogram of moisture spatial distribution of an agricultural field in Macomb, Illinois which was covered during the experiments. It is observed that although conventional coring techniques give an estimate of the average moisture of a vertical soil profile for a limited number of locations in a field, the moisture probe gives a better picture of within-field spatial variability of moisture. Such information along with other ground truth data served in the interpretation of remotely sensed radar and radiometric measurements.

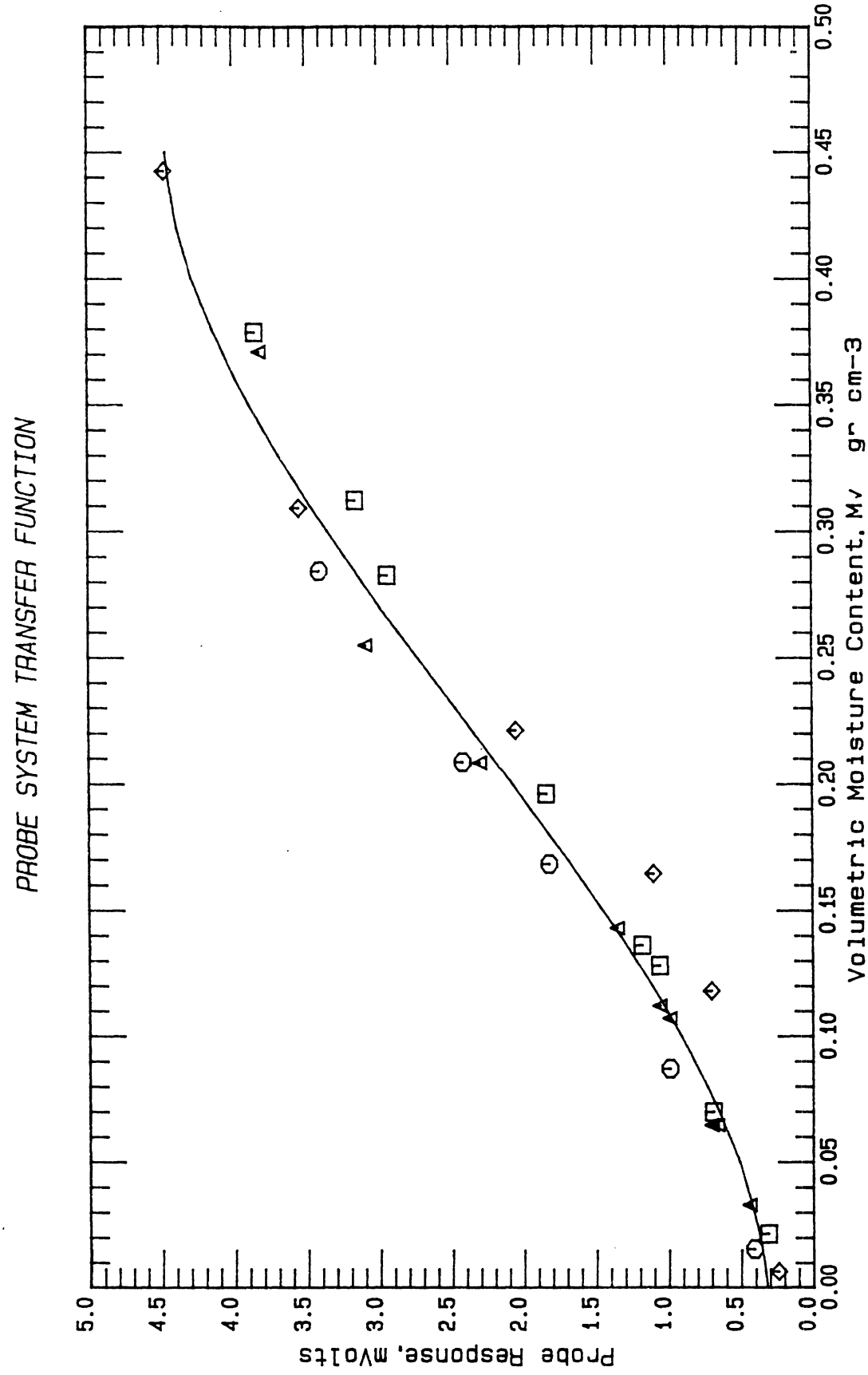

Figure 5.1: The soil moisture probe response for prepared soil samples of Table 2.1.

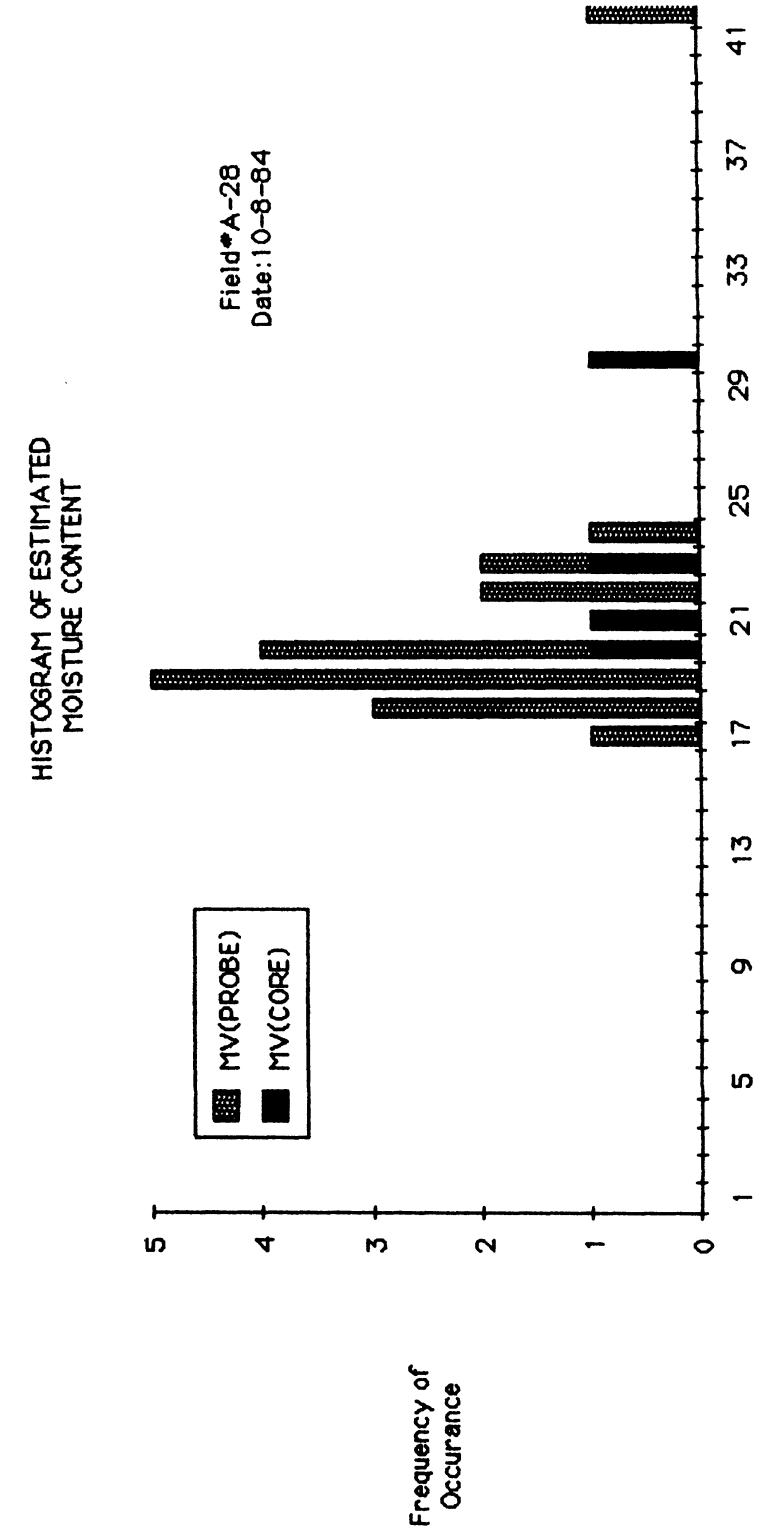

Figure 5.2: A histogram of estimated volumetric soil moisture in an agricultural field in Macomb, Illinois. The solid bars correspond to the samples processed in the lab.

Chapter 6

CONCLUSION

A simple and practical probe for detection of soil moisture operating at C-band was described. The system proved to be suitable for fast and repeatable field measurements with a precision of better than 5% regardless of the soil type. It was also shown that the moisture probe can be used effectively to study the spatial distribution of soil moisture in natural agricultural fields. A modified version of this system based on the reflection method is projected for direct measurement of the complex permittivity of materials by separating the phase and magnitude of the reflection coefficient.

Appendix A

THE LINEAR CAPACITANCE MODEL

Consider the Fresnel reflection coefficient $\Gamma = |\Gamma| \angle \phi$ for a dielectric medium of relative permittivity ϵ

$$\Gamma = \frac{Y_c - Y_L(\epsilon)}{Y_c + Y_L(\epsilon)} \tag{A.1}$$

where

$$Y_L(\epsilon) = G(\epsilon) + j\omega C_T(\epsilon) \tag{A.2}$$

and

$$C_T(\epsilon) = C_0\epsilon + C_f \tag{A.3}$$

$$G(\epsilon) = A\omega^4\epsilon^{2.5} \tag{A.4}$$

For proper choices of probe sizes and operating frequencies, the radiation loss may be neglected by setting $A = 0$. Thus, the simplified low-frequency (static)

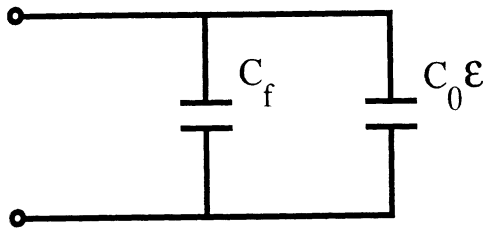

Figure A.1: The simplified model.

model is given by (Figure A.1)

$$Y_L(\epsilon) = j\omega(C_0\epsilon + C_f) \tag{A.5}$$

The validity of the proposed model for the admittance of the probe is contingent upon the following restrictions:

1. The model assumes a linear dependence between the capacitance of the probe and the permittivity of the medium. In other words, C_0 and C_f are assumed to be independent of permittivity and connected in parallel. This assumption has been shown to be valid for a wide range of high dielectric constant materials ($\epsilon' > 10$). However, even for $\epsilon' < 10$, the variations of C_0 and C_f with ϵ is relatively small and the linear model remains a very good approximation for all practical purposes.

2. In applying the above model, care must be taken to avoid the possibility of higher order mode propagation. This condition is satisfied when

$$\lambda_\epsilon > \frac{2(a-b)}{\gamma_1} \tag{A.6}$$

where $\lambda_\epsilon = \lambda_0/\sqrt{\epsilon'}$ is the wavelength in the medium, a and b are the outer and inner radii of the line, respectively, and

$$\gamma_1 = \frac{\chi_{01}}{\pi}(\frac{a}{b} - 1) \quad , \quad \chi_{01} = 1.36 \tag{A.7}$$

For standard semi-rigid cables $a/b = 3.27$, $\gamma_1 = 0.985$, and TM_{01} mode propagates if

$$\lambda_\epsilon \leq 2.03(a-b) \tag{A.8}$$

Therefore, as the dielectric constant of the medium ϵ' and/or frequency of operation increase, so does the possibility of higher order mode propagation. This is illustrated in Table A.1 for three standard air-filled coaxial lines $(a/b = 3.27)$ immersed in distilled water.

3. C_0 becomes frequency dependent at higher frequencies or when the dimensions of the line become comparable to the wavelength. Therefore, to ensure the frequency invariance of the probe capacitance, we require that

$$a/\lambda_o \ll 1 \tag{A.9}$$

This will also guarantee the static behavior of the probe by minimizing the radiation loss as discussed before.

Cable Size	TM_{01}-Mode Propagation ($\surd$)		
a, in.	$2.03(a-b)$	$f = 5$ GHz	$f = 10$ GHz
0.085	3.04	-	-
0.141	5.05	-	$\surd$
0.250	8.95	$\surd$	$\surd$

Table A.1: Higher order mode propagation for standard air-filled coaxial lines. The probes are assumed to be immersed in distilled water $\epsilon = 80 - j17.(a/b = 3.27, \lambda_\epsilon = 0.11\lambda_o)$.

An advantage of the linear model (A.5) is that it yields closed-form expressions for the real and imaginary parts of the relative permittivity in terms of the input reflection coefficient and frequency. Substituting (A.5) in (A.1) and solving for ϵ' and ϵ'', we obtain

$$\epsilon' = \frac{2|\Gamma|\sin\phi}{\omega Z_c C_0 [1 + |\Gamma|^2 + 2|\Gamma|\cos\phi]} - \frac{C_f}{C_0} \tag{A.10}$$

and

$$\epsilon'' = \frac{1 - |\Gamma|^2}{\omega Z_c C_0 [1 + |\Gamma|^2 + 2|\Gamma|\cos\phi]} \tag{A.11}$$

Clearly, the internal fringing capacitance C_f affects the value of ϵ' by the additive factor $Q = C_f/C_0$ and leaves ϵ'' unaffected. For example, if $Q = 0.2$, the error in calculation of ϵ' due to neglecting this factor for a medium of dielectric constant

$\epsilon' \geq 10$ is less than 2%

$$\frac{\Delta\epsilon'}{\epsilon'} \leq \frac{Q}{10} = \frac{0.2}{10} = 0.02 \tag{A.12}$$

It should be noted that C_f actually represents the upper limit of the internal fringing capacitance since the fringing fields tend to concentrate more into the dielectric material as the probe is inserted in the medium resulting in a lower value of effective fringing capacitance [13].

Appendix B

CALIBRATION PROCEDURE

The block diagram of the calibration setup comprising an automatic network analyzer is depicted in Figure B.1.

The accuracy of the measured reflection coefficient is affected by some well known nonideal effects in the calibration setup. This is shown in the signal flow graph of Figure B.2. The measured reflection coefficient Γ_m is given by

$$\Gamma_m = s_{11} + \frac{s_{12}s_{21}\Gamma_a}{1 - s_{22}\Gamma_a} \tag{B.1}$$

where Γ_a is the actual reflection coefficient; it is modified by the network analyzer's error terms which are identified as

s_{11}: *Directivity term* due to direct leakage of the incident signal into the reflectometer directional couplers,

s_{22}: *Source match term* caused by the mismatch between the connectors and the signal source, and

$s_{12}s_{21}$: *Frequency tracking and cross coupling term* due to frequency tracking and cross coupling in the forward and reflected measuring chambers caused by

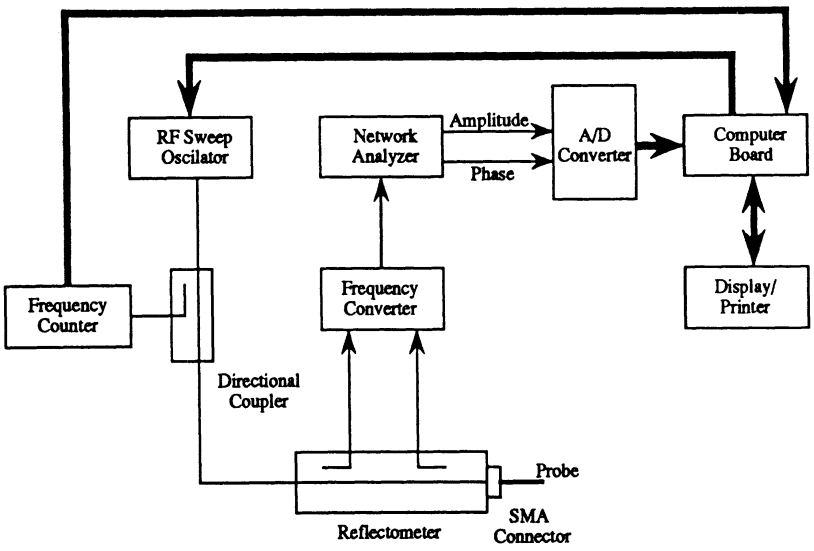

Figure B.1: Block diagram of the calibration setup.

small variations in gain and phase between the test and reference channels as a function of frequency.

A standard procedure using a combination of known calibration materials (different from that used for the calibration of the probe itself) can greatly improve the measured accuracy by eliminating the above nonideal effects. From (B.1), the corrected reflection coefficient is given by

$$\Gamma_m^c = \frac{\Gamma_m - s_{11}}{s_{22}(\Gamma_m - s_{11}) + s_{12}s_{21}} \tag{B.2}$$

which can be used to further improve the estimates of the probe equivalent circuit components.

The calibration algorithm shown in Figure B.3 was implemented to estimate the equivalent circuit components. The standard loads used were open circuit, short circuit (the probe immersed in mercury), distilled water, and methanol. The

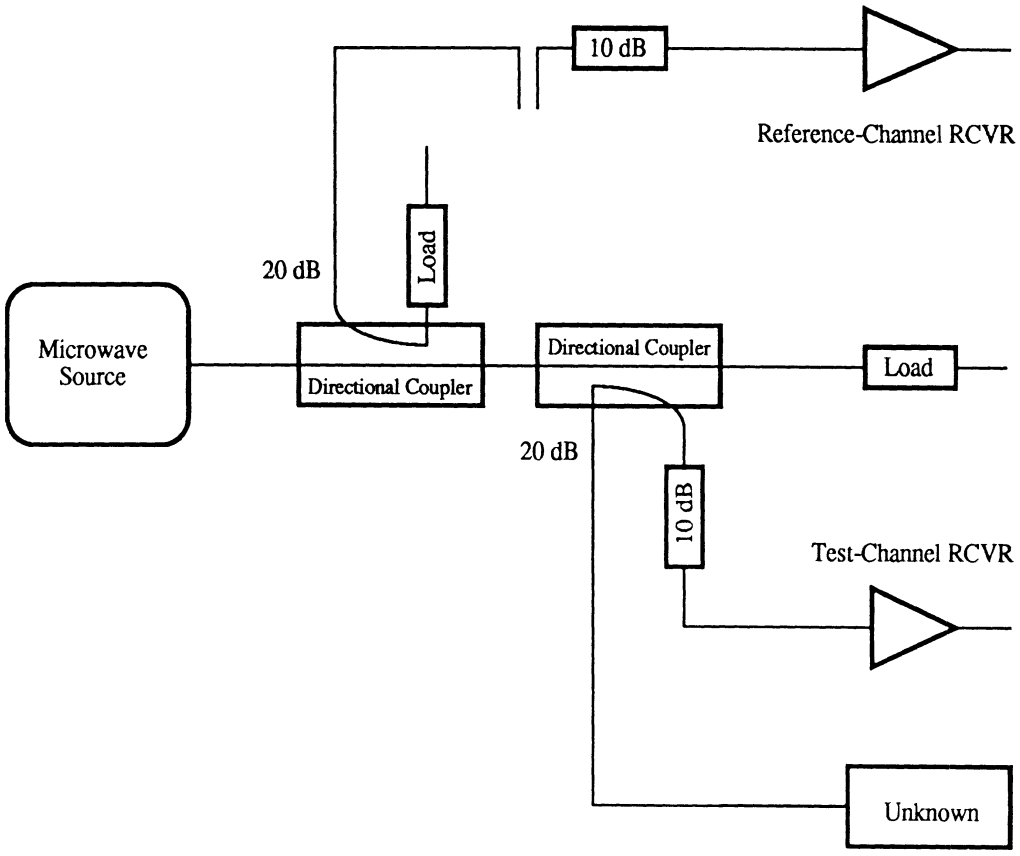

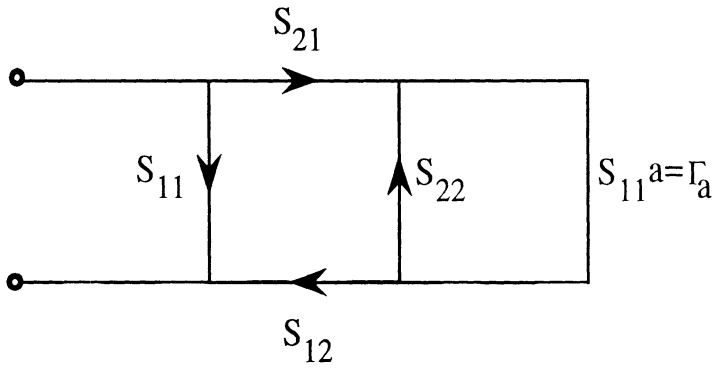

Figure B.2: Signal flow graph of error terms.

summary of results obtained for the 0.085″ coaxial line is shown in Table 4.1.

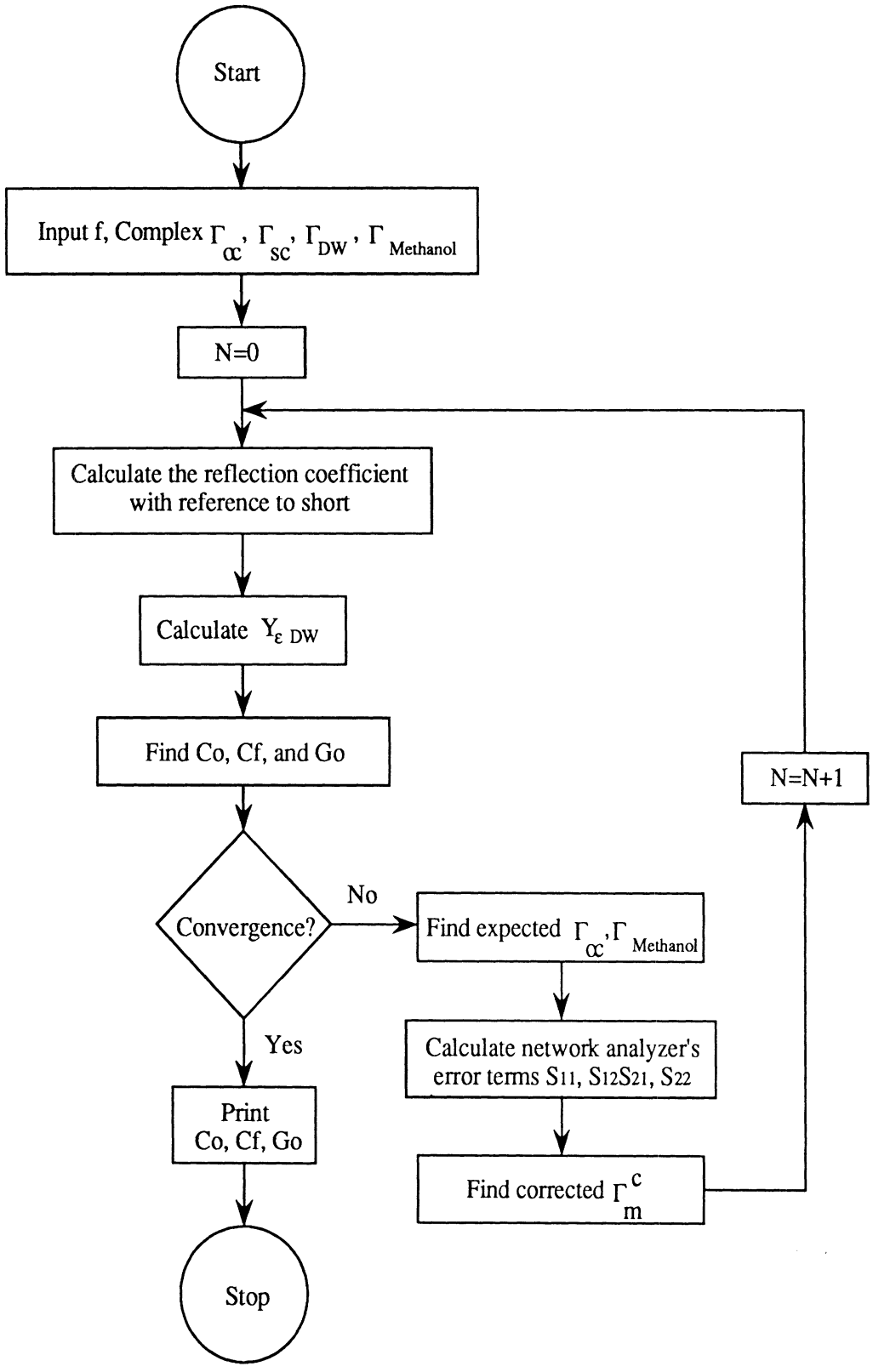

Figure B.3: Calibration algorithm.

Appendix C

MICROSTRIP CIRCUIT DESIGN

A 1.5λ circular ring with four ports separated by 60° angles makes a rat-race coupler or a 180° hybrid ring (Figure C.1). The four ports are separated by $\lambda/4$ and $3\lambda/4$, with λ being the wavelength in the transmission medium

$$\lambda = \frac{c}{f_o\sqrt{\epsilon_{re}}} \tag{C.1}$$

where c is the speed of light, f_o is the operating frequency, and ϵ_{re} is the effective dielectric constant of the microstrip given by

$$\epsilon_{re} = \frac{\epsilon_r + 1}{2} + \frac{\epsilon_r - 1}{2}(1 + 10\frac{h}{w})^{-1/2} \tag{C.2}$$

in which ϵ_r and h are the substrate dielectric constant and thickness, respectively and w is the microstrip line width.

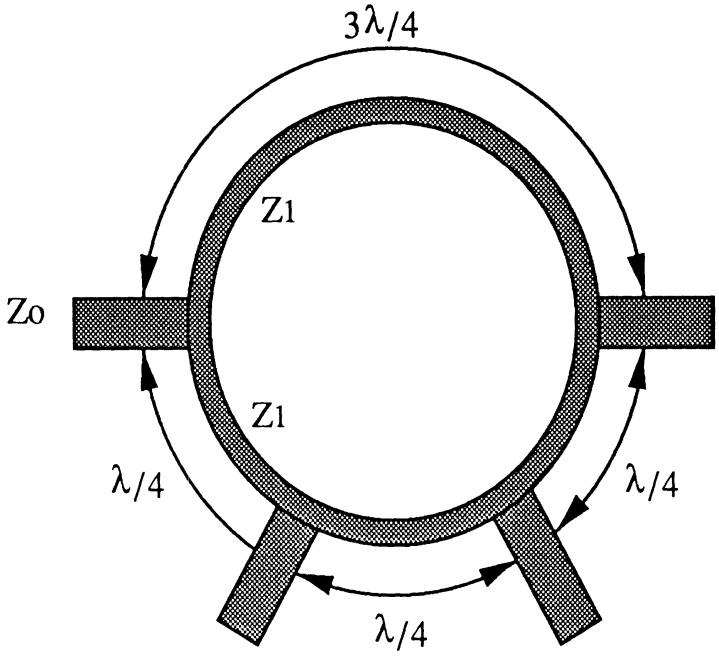

Figure C.1: The 3 dB hybrid 180° rat-race coupler.

The scattering matrix for the ideal rat-race can be written as

$$S = \begin{bmatrix} 0 & s_{12} & 0 & s_{14} \\ s_{21} & 0 & s_{23} & 0 \\ 0 & s_{32} & 0 & s_{34} \\ s_{41} & 0 & s_{43} & 0 \end{bmatrix} \tag{C.3}$$

For an equal split in power (3 dB rat-race) all non-zero scattering coefficients are $1/\sqrt{2}$ and from power considerations, we may write

$$(\frac{1}{Z_0})^2 = 2(\frac{1}{Z_1})^2 \tag{C.4}$$

and thus

$$Z_1 = Z_0\sqrt{2} \tag{C.5}$$

The synthesis steps are as follows:

1. Choose a port impedance Z_0,
2. Calculate Z_1 from (C.5),
3. Find ϵ_{re} from (C.2),
4. Use (C.1) to find λ, and
5. Calculate the line width for the ring from semi-empirical relations [14].

Also, in order to take the effect of discontinuities into account, three cases were considered in the process:

- Uncompensated lengths without discontinuities,
- Discontinuities taken into account to estimate the degree of degradation of the circuit performance,
- Incremental reduction in the line lengths to compensate for the inductances caused by the discontinuities.

The specifications of the microstrip substrate used were as follows

$$h = 0.030'' \quad , \quad \epsilon_r = 2.45 \quad , \quad t = 0.0014'' \tag{C.6}$$

The rat-race was analyzed by a computer aided approach utilizing existing models for the T-junctions and discontinuity models [14]. The design parameters of the ring are ($f_o = 5$ GHz)

$$Z_0 = 50\Omega \quad w = 0.0840'' \quad \epsilon_{re} = 2.06 \tag{C.7}$$

$$Z_1 = 70.71\Omega \quad w = 0.0467'' \quad \epsilon_{re} = 1.98 \tag{C.8}$$

$$\begin{aligned} \ell_c &= \frac{\lambda_o}{\sqrt{\epsilon_{re}}}(\frac{1}{4} - \Delta\ell) \quad , \quad \Delta\ell = 2.5\% \\ &= 0.959cm \end{aligned} \tag{C.9}$$

where ℓ_c is the corrected length for the quarter wavelength separation between the coupler ports.

Figures C.2-C.5 show the simulated performance of the hybrid coupler under both ideal and nonideal assumptions.

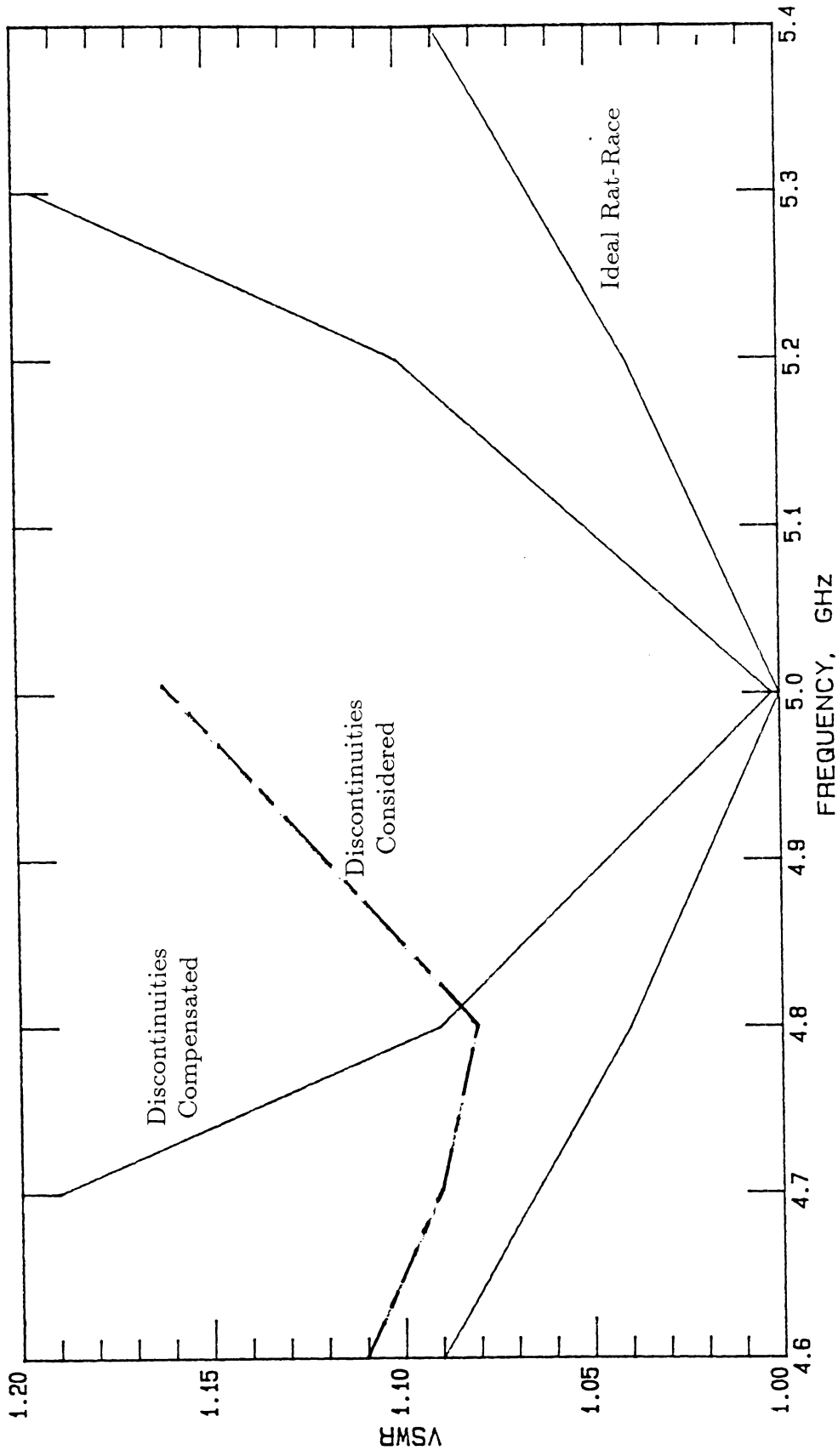

Figure C.2: The calculated VSWR for the rat-race with and without discontinuity compensation.

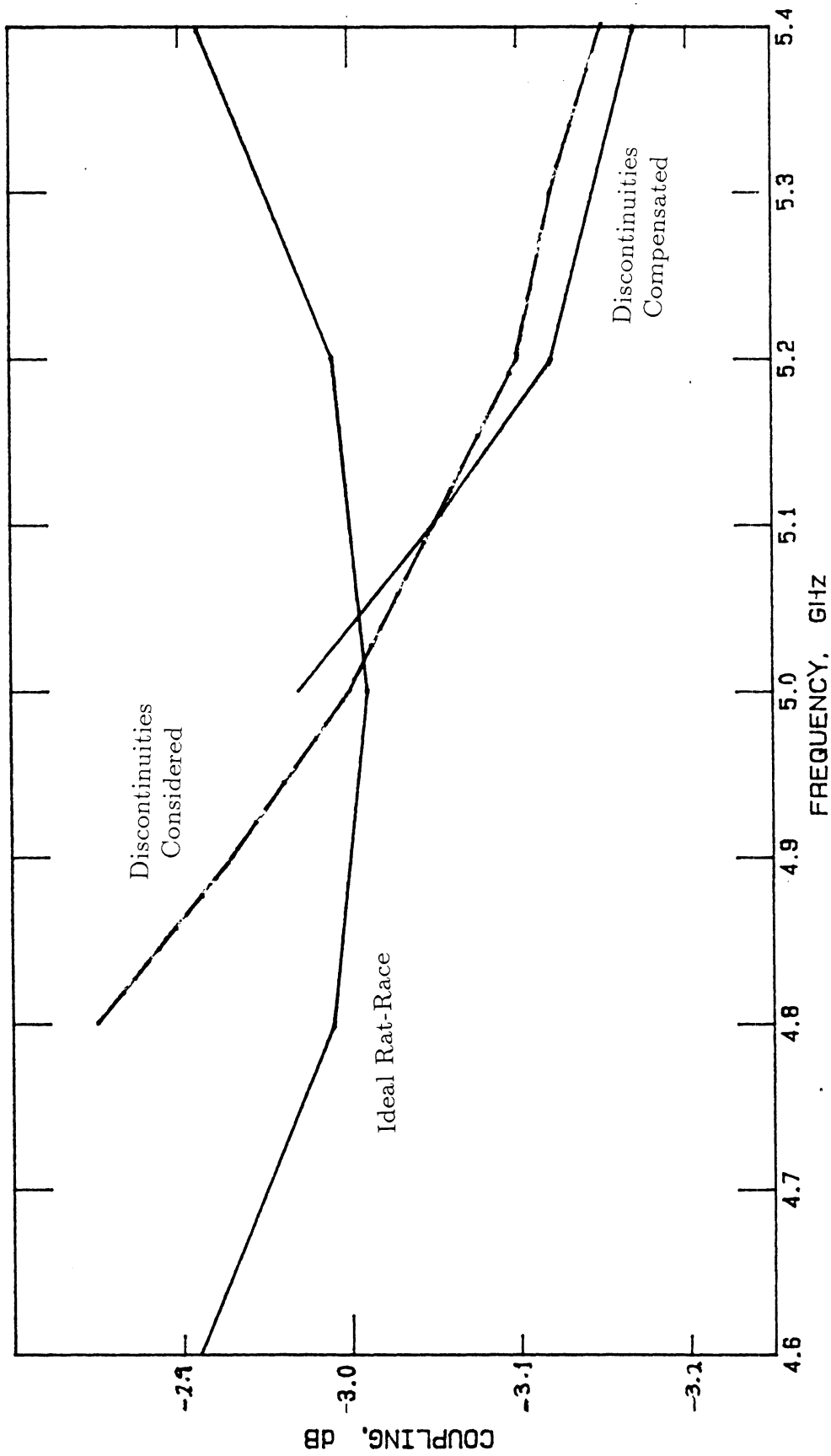

Figure C.3: Rat-race coupling.

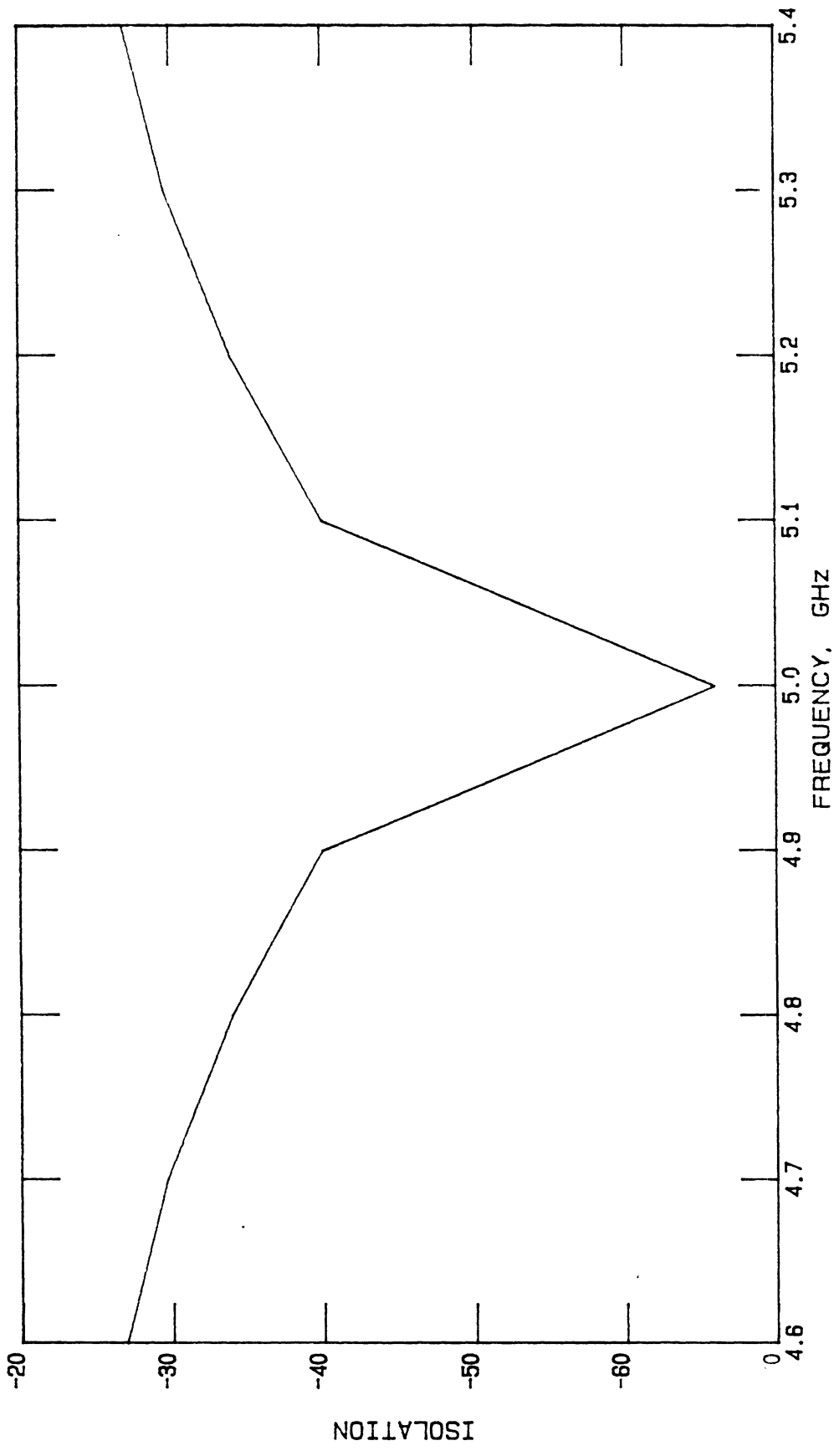

Figure C.4: Rat-race isolation.

Bibliography

[1] G. S. Smith and R. W. P. King,"The resonant linear antenna as a probe for measuring the in-situ electrical properties of geological media," *J. Geophysical Res.*, vol. 79, no. 17, pp. 2623-2628, June 1974.

[2] J. L. Davis, "Relative permittivity measurement of sand and clay soil in-situ," *Geol. Surv. Can.*, paper 75-1C, pp. 361-365.

[3] M. A. Stuchly, S. S. Stuchly, "Coaxial line reflection methods for measuring dielectric properties of biological substances at radio and microwave frequencies– A review," *IEEE Trans. Instrumen. Meas.*, vol. IM-29, no. 3, pp. 176-183, Sept. 1980.

[4] C. M. Dobson, K. Barkeshli, F. T. Ulaby and D. Brunfeldt, "A microwave dielectric probe for in-situ measurement of soil moisture," *Fourth International Symposium on Remote Sensing and Soil Survey*, Gavaringen,The Netherlands, March 4-5, 1985.

[5] F. T. Ulaby, R. K. Moore, A. K. Fung, *Microwave Remote Sensing, Active and Passive,* Norwood, Artech House, 1986, volume 3, appendix E, p. 2090.

[6] J. R. Birchak, C. G. Gardner, J. E. Hipp, and J. M. Victor, "High dielectric constant microwave probes for sensing soil moisture," Proc. IEEE, vol. 62, no. 1, pp. 93-98, Jan. 1974.

[7] N. Markuvitz, *Waveguide Handbook*, Dover, New York, 1965, p. 213.

[8] G. B. Gajda, S. S. Stuchly, "Numerical analysis of open-ended coaxial lines," *IEEE Trans. Microwave Theory Tech.*, vol. MTT-31, no. 5, pp. 380-384, May 1983.

[9] T. W. Athey, M. M. Stuchly, S. S. Stuchly, "Measurement of radio frequency permittivity of biological tissues with an open-ended coaxial line: part I," *IEEE Trans. Microwave Theory Tech.*, vol. MTT-30, no. 1, pp. 82-92, Jan. 1982.

[10] G. A. Descahmps, "Impedance of an antenna in a conducting medium," *IRE Trans. Antennas Propagat.*, Sept. 1962, pp. 648-650.

[11] M. Hallikainen, F. T. Ulaby, M. C. Dobson, M. El-Rayes, and L. K. Wu, "Microwave dielectric behavior of wet soil–Part I: Empirical models and experimental observations," *IEEE Trans. Geosci. Remote Sensing*, vol. GE-23, no. 1, pp. 25-34, Jan. 1985.

[12] M. C. Dobson, F. T. Ulaby, M. Hallikainen, M. El-Rayes, "Microwave dielectric behavior of wet soil–Part II: Dielectric mixing models," *IEEE Trans. Geosci. Remote Sensing*, vol. GE-23, no. 1, pp. 35-46, Jan. 1985.

[13] M. F. Iskander, S. S. Stuchly, "Fringing field effect in the lumped-capacitance method for permittivity measurement," *IEEE Trans. Instrumen. Meas.*, vol. IM-27, no. 1, Mar. 1978.

[14] K. C. Gupta, R. Garg, R. Chadha, *Computer-Aided Design of Microwave Circuits*, Artech House, 1981.